Sensors & Actuators: B. Chemical 345 (2021) 130010

Contents lists available at ScienceDirect

Sensors and Actuators: B. Chemical

journal homepage: www.elsevier.com/locate/snb

Hygroscopicity Enhancement of Low Temperature Hydrothermally Synthesized Zinc Oxide Nanostructure with Heterocyclic Organic Compound for Humidity Sensitization

Muhammad Arif Riza [a], Yun Ii Go [a,*], Robert R.J. Maier [b], Sulaiman Wadi Harun [c], Siti Barirah Ahmad Anas [d]

[a] School of Engineering and Physical Sciences, Heriot-Watt University, Malaysia1, Jalan Venna P5/2, Precinct 5, 62200, Putrajaya, Malaysia
[b] Institute of Photonics and Quantum Sciences, Heriot-Watt University, Edinburgh, Scotland, EH14 4AS, United Kingdom
[c] Department of Electrical Engineering, University of Malaya, Kuala Lumpur, 50603, Malaysia
[d] Wireless and Photonics Networks Research Centre, Faculty of Engineering, Universiti Putra, Malaysia

ARTICLE INFO

Keywords:
Additives
Humidity
Hydrothermal
Hygroscopic
Zinc oxide

ABSTRACT

Materials that have hygroscopic capabilities are potent sensing elements for humidity sensors. The hygroscopic behaviour of zinc oxide (ZnO) with modified nanostructure was synthesized and characterized. Heterocyclic additive was added on ZnO to improve its hygroscopic capability for humidity sensitization. ZnO capability of water molecule adsorption was tested with a hygroscopic characterization method adapted from American Society for Testing and Materials (ASTM) method for hygroscopic determination. It was found that inclusion of additive improves the water retention and release ZnO, making it more viable for use in sensors that take advantage of mechanical strain due to weight for humidity determination. The hygroscopic behaviour was observed in the steeper gradient on the mass change during humidity exposure to the ZnO compound with the additive compared to non-additive ZnO. Furthermore, the additive loaded ZnO showed greater reliable regression, R2 value (3.56 %) compared to the non-additive ZnO sample. Crystal analysis via X-ray diffraction (XRD) revealed increment on ZnO characteristic peaks (002) and (101) upon addition of the organic compound to the ZnO which influence the nanostructure of the material. Field emission scanning electron microscopy (FESEM) indicates porous and hemispherical nanostructure. Elemental analysis showed minimal impurities present on both ZnO and additive loaded ZnO. The hygroscopic capabilities of ZnO synthesized with low temperature hydrothermal technique allows for implementation in many humidity sensing options required by industries of various fields.

1. Introduction

In material studies, hygroscopicity is the ability of a material to allow water molecules to be absorbed into or desorb out of itself [1]. Materials that have high hygroscopic properties absorbs moisture and have the potential to be adopted into environmental sensing technologies. Factors that influence the hygroscopicity of the material depends on several factors which are surface area of the material coating and hydrophilicity of the chemical groups involved in the material compound [2,3]. Hygroscopic materials such as polymers, soluble crystals, salts that have rough nanostructures are bound to have hygroscopic nature. Measuring the hygroscopic capabilities of materials may assist in development or innovation of sensors for the detection of water molecules in the environment.

1.1. Hygroscopic materials and diffusion

Hygroscopic capability of a material relates to diffusion of water molecules into the said material.

Since water is a polar vapor, it would not follow rules of physisorption which is the accumulation of non-polar chemicals such as O_2, CO_2 and CH_4 on the solid surfaces. Therefore, physisorption integration with the Fick's law model is neglected [6]. Water does not react in the molecular level when in contact with ZnO surface under ambient

* Corresponding author.
E-mail address: y.go@hw.ac.uk (Y.I. Go).

https://doi.org/10.1016/j.snb.2021.130010
Received 25 February 2021; Received in revised form 26 March 2021; Accepted 18 April 2021
Available online 20 April 2021

Table 1
Hygroscopic techniques.

Technique	Ref.
Weighing method	[9,10,11]
Simulation with real environment data	[12]
Tandem nano-differential mobility analysis (TDMA)	[13]
Microscopic observation	[14,15,16,17]
Sum of frequency generation spectroscopy (SFG)	[18]

Table 2
Other hygroscopic analytical techniques.

Technique	Output data form/ Performance parameter	Key Finding and research gap	Ref.
Micro droplet test	Interfacial stress value and shear strength monitored in various RH% via micro-bond system.	• Obtained a relationship between strength and stress of material against various RH% • Load imposed to material during stress test is reported.	[19]
Sample stress measurement with extensometer	Comparison of height of sample film and hygroscopic stress change values	• Samples were in form of large size cylinders to be able to measure its stress via extensometer. • Hydrophilicity and pH neutralization of material was presented but no display of nano-structural images.	[20]
Surface thickness profiling	Comparison of height of sample film before and after water immersion	• Results were discussed on sample height changes in relation to its hygroscopicity only. No weight comparison and microscopy report.	[21]
Sample volumetric change monitoring via laser scan micrometer (LSM) system	Comparison of sample volume size before and after water immersion.	• Reported only on solid samples with actual 3-dimensional shape. • No microscopic images on nanostructure	[22]
Hyperbolic representation adsorbed water content against time exposed to 100 % RH	Hyperbolic plots of soil to exposure time of 100 % RH	• Reported results only on soil samples and exposed with 100 % RH (addition of water). • No microscopic images	[23]
Tandem nano-differential mobility analysis (TDMA)	FTIR, Growth factor curve, NMR spectroscopy	–	[13]
Sum of frequency generation spectroscopy (SFG)	SFG, ATR-IR	–	[18]
Weighing technique (this study)	Sample weight, FESEM, EDS, XRD	• Improved technique for hygroscopicity determination between material films. • Has potential to be applied with other materials as long as in thin film form. • Serve as an effective and calibrated method for testing hygroscopicity of material nanostructures.	–

temperature and pressure. Therefore, chemisorption models will also be neglected since this phenomenon only applies to adsorbate and adsorbent having altered chemical bonds during reaction that caused the adsorption which are temperatures beyond 400 °C and ultra-high vacuum state [7,8]. Another related adhesion phenomenon would be condensation of water molecules on to the zinc oxide surface. According to Byrn, et al. [6], condensation of water on to a surface can only happen spontaneously at relative humidity of no less than 100 %. Observing and testing the hygroscopicity of a material can be done with different techniques. Tables 1 and 2 show different techniques implemented by other studies for material hygroscopic testing in terms of the parameters involved and sample form.

1.2. Zinc oxide nanostructure

Zinc oxides are one of the common materials used in wide variety of applications. Aside from its electrical properties such as wide band gap and magneto-resistance, its physical and chemical properties have pulled interest of many researchers as well. Nano-structural modifications are possible to be applied during synthesis of ZnO. Besides using completely different synthesis routes to produce ZnO, slightly manipulating separate process parameters during synthesis may cause its nanostructures to change. One of the most significant ZnO functionalized nanostructure was achieved with low temperature growth technique and additives leading to nanowire form and nanoforest form with large surface area for solar cell applications [24,25]. Studies utilize zinc oxide as part of their sensing element in sensors such as dopamine detector [26], pH sensor [27] and butylamine sensors [28] as shown in Fig. 1.

1.3. Hexamethylenetetramine (HMT) influence on a material nanostructure

While various studies reported on use of HMT with ZnO, this does not mean the additive is only tied to be used with a specific metal precursor. HMT was seen used in other studies involving transitional metal oxides such as TiO_2 [31], WO_3 [32] and CuCn [33]. The structure influencing effect of HMT varies from different materials that it is used with. In a study by Umar, et al. [34], copper oxide nanostructures were modified with the addition of HMT. The HMT assisted hydrothermal synthesis of copper oxide has led to formation of nano-sheet shapes of the copper oxide nanostructure. Han, et al. [35] mentions that HMT influence growth rate of In_2O_3 nanobricks in a way that results in fast formation of crystal growth due to increasing OH- ions formed from the dissolution of HMT. When at higher concentrations, the accelerated formation of crystal growth rate forms irregular crystals. Therefore, concentration of HMT should be kept low to maintain crystal and nanostructure. When applied with zinc source precursors, structures such as needle or rod shaped are more predominant. There are many studies [36–40] involved the use of HMT in conjunction with zinc oxide to influence nanostructure and assist its synthesis process. In producing zinc oxides, various precursors of zinc are available which are the acetates, nitrates and chlorides. HMT is frequently reported with its use with nitrates due to ability to produce nanorod shaped structures suitable mostly in photovoltaics. Acetates of zinc have been reported to form hemisphere or cabbage like structures of high surface area suitable for adsorption and desorption of chemicals and anti-bacterial effects [41]. Chloride salt of zinc tend to produce plate like nanostructures at low temperatures [42]. It is common among these studies to use equimolar or reduced amounts of HMT with their zinc precursors.

1.4. Humidity sensing and hygroscopicity of materials

The hydrophilicity and hygroscopicity of materials allow potential use as a humidity sensor. The deformation that occurs upon water uptake of a nanomaterial can be utilized to form a sensor up to a certain

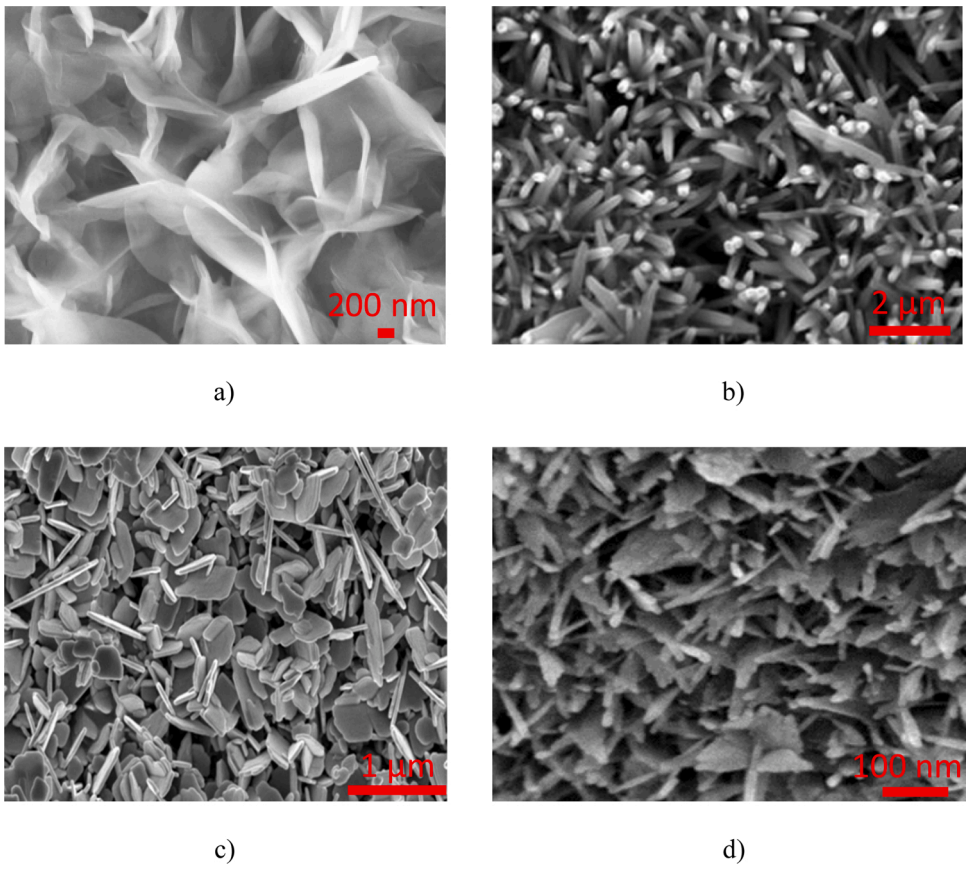

Fig. 1. Potential nanostructures of Zinc Oxides; a) Nanowalls/crease [27], b) Nano rods [29], c) Nanoflakes [28] and d) Rod and flake hybrid [30].

degree. Reversibility of the deformation before and water uptake determines the reliability of the said sensor. Optical based sensors with their robustness, flexibility and electromagnetic resistive properties [43] are suitable to be used with chemical coatings. Many studies have taken advantage of hygroscopic materials capability to produce a sensor. For instance, Caponero, et al. [44], utilized polymer coatings on a fiber Bragg grating (FBG) based optical sensor. The hygroscopic polymer was coated on the sensor mechanism of the FBG that produce perturbed signals upon induction of strain by the hygroscopic coating upon humidity exposure. The incorporation of hygroscopic polymer with the sensing mechanism of an optical FBG sensor allows for a compact and sensitive humidity detection even within small crevices of an object.

2. Methodology

This section discusses the synthesis of the zinc oxide nanostructure and deposition of the material on to a substrate slide. It also covers the method of hygroscopic characterization for zinc oxide and HMT enhanced zinc oxide.

2.1. Materials and zinc oxide film synthesis

The main synthesis precursor material is zinc acetate dihydrate ($ZnAc_2$). HMT is the surfactant used for the modification of the nanostructure. The role of HMT is to modify the surface tension of the solvent and further contributes the release of OH^- ions for ZnO growth [41]. Therefore, implementation of this additive is with $ZnAc_2$ instead of zinc nitrate which was often used with HMT in other studies [36–40]. For humidity manipulation, Sodium hydroxide and silica beads were used. Glass slides were used as the substrates for the films.

Zinc oxide synthesis follows a method of modified hydrothermal route. Fig. 2 shows the flow of the synthesis route. This method involves in precursor solution of zinc acetate dissolved in ethanol. The solution was stirred continuously with magnetic bar to form a ZnO nanoparticle solution. The resulting solution was stirred further with the addition of NaOH which acts as a structure crystal influencer and promotes additional supplies of hydroxyl ions (-OH). The additional hydroxyl ions react with the Zn^{2+} ions forming a whitish solution of $Zn(OH)_2$. The solution was then sonicated to allow the precursor to mix well and forms a growth solution. The solution was dropped onto a thin microscopic glass slides before proceeding to be annealed in an oven. Annealing proceeded for two hours at low temperature of 70 °C. The samples were ready to be tested for hygroscopicity after the annealing process. The overall reaction mechanism of the ZnO route:

$$Zn(CH_3COO)_2 \text{ -> } Zn^{2+} + CH_3COO^2 \text{ (Dissolution reaction)} \quad (6)$$

$$NaOH \text{ -> } Na^{2+} + 2OH^- \quad (7)$$

$$Zn^{2+} + 2OH^- \text{ -> } Zn(OH)_2 \quad (8)$$

$$Zn(OH)_2 \text{ -> } ZnO + H_2O \text{ (ZnO Nanoparticle formation)} \quad (9)$$

2.2. HMTA enhanced zinc oxide synthesis and hygroscopic test

Zinc oxide with added additive also proceeds the same synthesis route as mentioned. However, at the stage of the addition of NaOH, 0.1 M of HMTA was also added. The HMTA acts as a nanostructure modifier supporting NaOH for forming zinc oxide growth solutions. The deposition and annealing methods were the same as the zinc oxide.

For comparing the hygroscopicity between ZnO and ZnO-HMT, method of weigh comparison between two materials upon humidity exposure is applied. Set up is visualized in Fig. 3. The thin film of ZnO was weighted during exposure to initial humidity which was set to 30 %

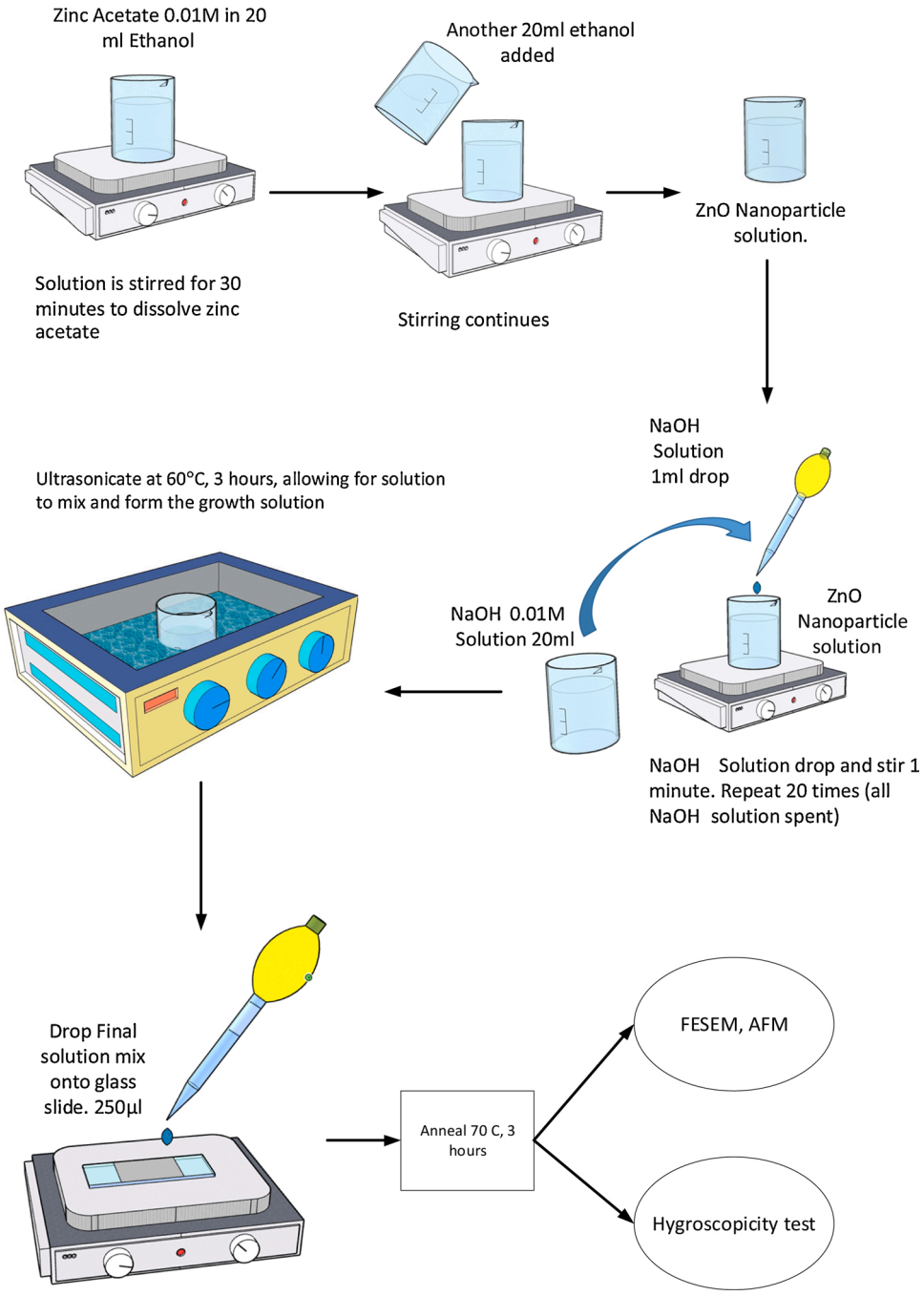

Fig. 2. Synthesis route of ZnO.

RH within an enclosed chamber placed on mass balance. Humidity within the chamber is raised by adding NaOH dissolved in water at a separate compartment within the chamber. At every 10 % RH raised, the mass of the sample is recorded until 80 % RH. The difference of mass at each humidity is an indication that the sample material has absorbed and accumulated water molecules within its structure thus raising its weight, albeit very slightly. Upon reaching 80 % RH, the humidity modifier substance was swapped with silica beads to reduce the moisture within the enclosure. Mass of the sample was recorded the same way as during the increment of the relative humidity to verify whether desorption of water molecules can happen and allow the sample to regain its original weight. Temperature during humidity measurement recorded with temperature module included with the humidity sensor was 29 °C at first ten minutes and stable at 23 °C throughout the operation. The procedure was repeated with ZnO-HMT thin film to compare with the basis ZnO thin film. Fig. 4a) shows the actual testing setup and Fig. 4b) is how the sample is stored within a sealed container with silica beads inside for reducing moisture within.

2.3. Potential fabrication of ZnO-HMT based humidity sensor

To take advantage of the hygroscopic nanostructure of zinc oxide, a suitable mode of sensing to be used should be chosen. Since ZnO can act as a hygroscopic material that deforms upon intake and outtake of water, FBG sensing mechanism is viable. FBG sensors rely on the micro strain of the grated cores. The coating of the ZnO-HMT follows the dip and dry method. The FBG segment of a fiber was immersed within a ZnO-HMT solution and dried. After repetition of the steps for at least 10

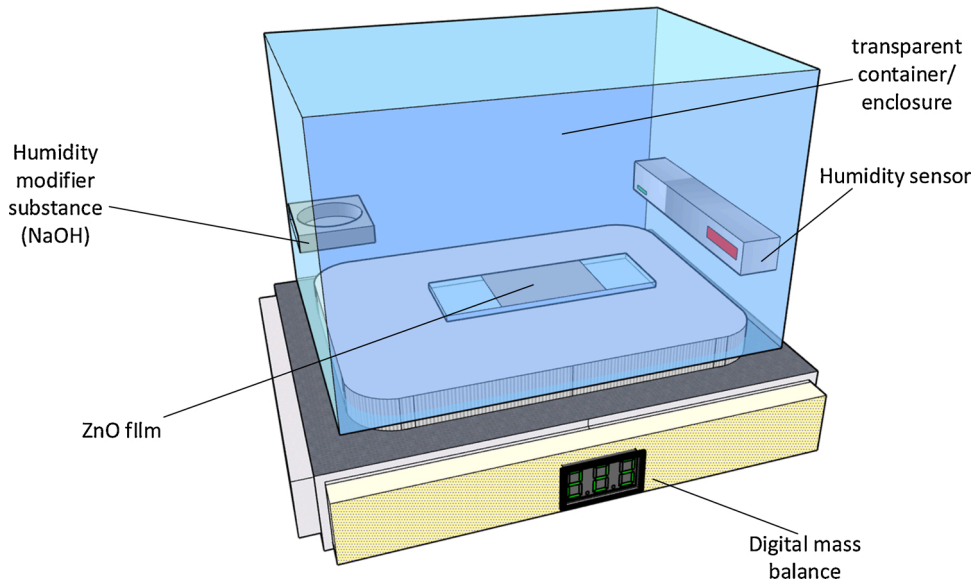

Fig. 3. Hygroscopic test chamber.

Fig. 4. a) actual experimental setup and b) sample storage.

times, the coated FBG was annealed to allow the development of the zinc nanostructure. With connection with a source and optical transducer, data on humidity sensing can be produced.

2.4. Material characterization

Upon completion of material synthesis, characterization was performed to validate whether the preferred synthesized material was formed and presence of impurities. Crystal structure of the material was analysed via Bruker D8 Advance XRD equipment with CuKα radiation source with 2θ scanning angle range of 0̊until 80̊. Material morphology was done with Merlin Compact FESEM with added elemental dispersive spectroscopy (EDS) for elemental analysis.

3. Results and discussion

3.1. Hygroscopicity characterization of ZnO/HMT

Upon testing of hygroscopicity via microbalance of ZnO. Hygroscopic properties can roughly be seen at increasing humidity. Increment of humidity is nearing to a halt upon reaching 80 % RH which marks the material having absorbed close to its maximum capacity. At this point, the film has shown notable droplets of water present on its surface. Fig. 5 shows this hygroscopic phenomenon. When reducing the humidity from 80 % back to 40 % RH via chemically forced drying with $CaCl_3$. RH is seen decreasing slightly slow and returning to approximately 50 % RH. Upon returning to 50 % RH, only minimal amounts of water droplets still exist on the surface of the material. If dried longer it is possible that the mass of ZnO thin film will return to its original value. Relating this phenomenon with Crank's approach in equation (5), the uptake of water, M_t would be mass of the water that are adhered onto the glass slide upon exposure to humidity and M_E would be the mass of the substrate and chemical coating equilibrium state. The equilibrium state is in which the RH is most stable (50 %RH) and act as basis of this observation.

Upon recording the mass of the samples within a closed chamber, Fig. 6a) and b) were plotted according to values in Table 3. Based on both Fig. 6a) and b), it is worth noting that both samples exhibit

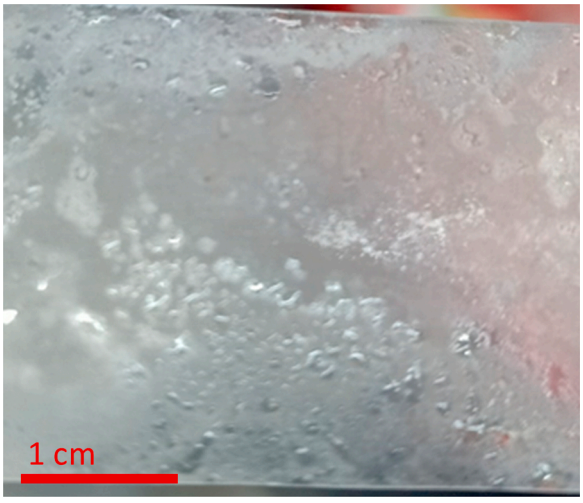

Fig. 5. Water droplets present on surface of film upon exposure to high humidity (>70 %RH).

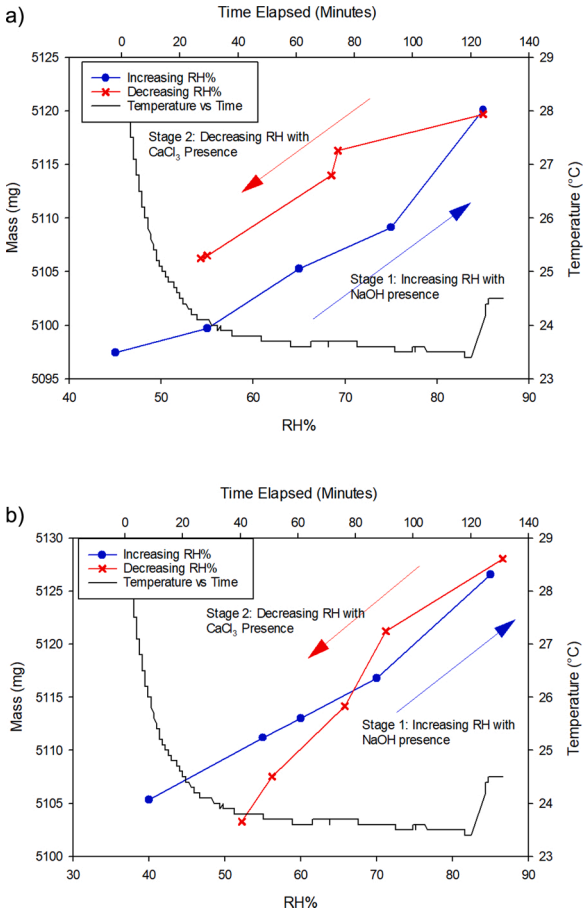

Fig. 6. Weight vs humidity of a) ZnO and b) ZnO-HMT.

hygroscopic behaviour when the mass changes upon introduction and reduction of humidity. Along with the main curves, the recorded temperature was also plotted. Temperature during the test remains between 24 °C and 27 °C. The steep temperature reduction from 0–3 minutes may be due to the preparation process (positioning of the sample, humidity source, sensor and etc.) of the chamber as the datalogger used to record the temperature was already turned on in order to monitor the chamber temperature. ZnO-HMT can be seen having slightly improved

Table 3
Incrementing and decrementing RH and mass values average for ZnO and ZnO-HMT.

ZnO				ZnO-HMT			
Incrementing RH		Decrementing RH		Incrementing RH		Decrementing RH	
RH (%)	Mass (mg)	RH (%)	Mass (mg)	RH (%)	Mass (mg)	RH (%)	Mass (mg)
45.0	5097.46	85.0	5119.70	40.0	5105.33	86.6	5128.04
55.0	5099.71	69.2	5116.30	55.3	5111.20	71.2	5121.22
65.0	5105.29	68.5	5114.00	60.0	5113.02	65.8	5114.17
75.0	5109.15	55.0	5106.50	70.1	5116.78	56.2	5107.52
85.0	5120.11	54.3	5106.25	85.0	5126.56	52.2	5103.29

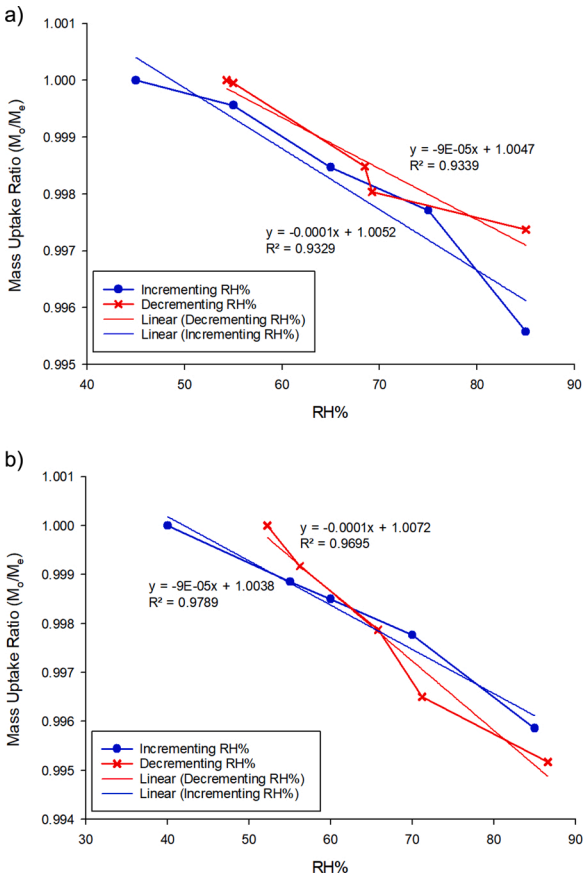

Fig. 7. Mass uptake ratio of a) ZnO and b) ZnO-HMT.

water uptake and water release during increment and decrementing of RH. The improvement is in the steepness of the curve with the mentioned sample having steeper curve compared to the sample without the additive.

While the curves in Fig. 6 is still vague in nature when presented, Fig. 7a) and b) were plotted with ratio of sample mass at lowest RH% to mass of sample at exposed certain RH%. This was done to observe how much mass change in comparison to the weight of the sample at its driest state. Higher gradient depicts that mass change is observed upon humidity increase. In Fig. 7a) ZnO incrementing RH curve overlaps twice with the decrementing curve. This could cause discrepancy of data when the material is used for humidity sensing as it does not change mass at certain point in humidity and follow the trend of linear proportion of humidity and sample mass. In Fig. 7b), the curves seem much smoother with only one intersection of curves. This could be concluded that ZnO-HMT poses more consistent water retention and water release capability.

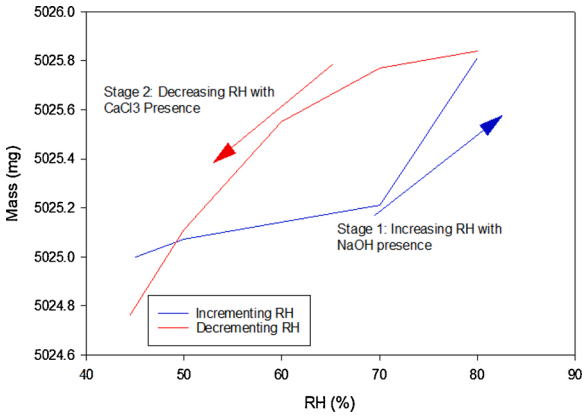

Fig. 8. weight vs. humidity curve of a blank glass slide.

A blank glass slide that is not coated with ZnO or ZnO-HMT was also tested for comparative purpose. Since water molecule adhesion can occur to almost anything with a surface, it is worth to observe the hygroscopic curve through the weighing technique. Fig. 8 shows the weight versus humidity curve a blank glass slide exposed to incrementing and decrementing humidity. Low gradient is observed on stage 1 of the test which depicts a very poor water adhesion differences at each humidity increase. At RH 70%–80% a steep increase occurred which may be due to larger droplets finally forming from the many small water molecules attached. At stage 2 the reduction of water mass from high RH to lower RH also has a low gradient throughout all the temperature ranges. The water molecule decrement at every RH interval looked more natural compared to stage 1.

3.2. *Surface morphology*

FESEM observation results have been made on both samples after the

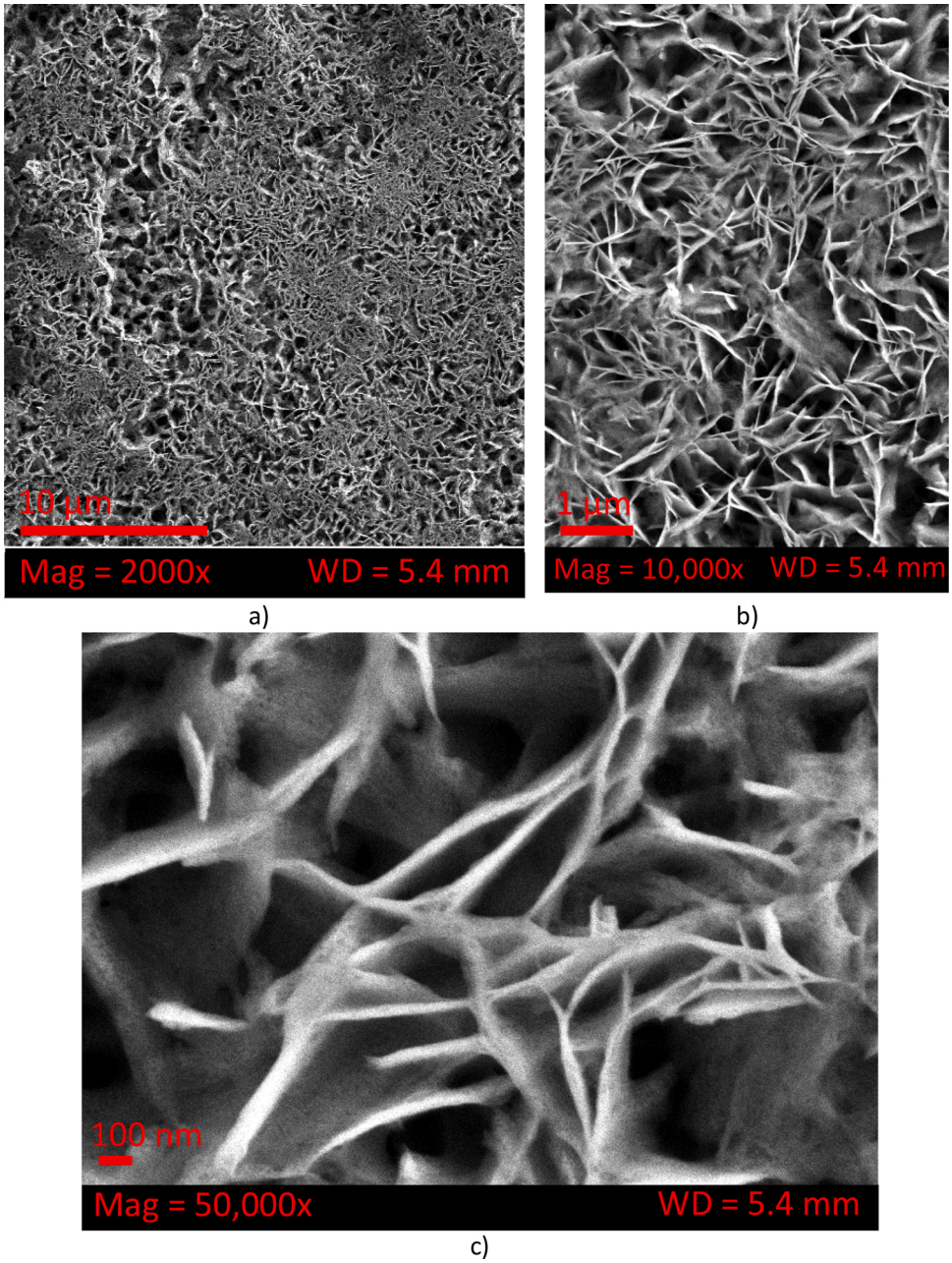

Fig. 9. FESEM Images of ZnO at various magnifications – a) 2000x magnification, b) 10,000x magnifications and c) 50,000x magnifications.

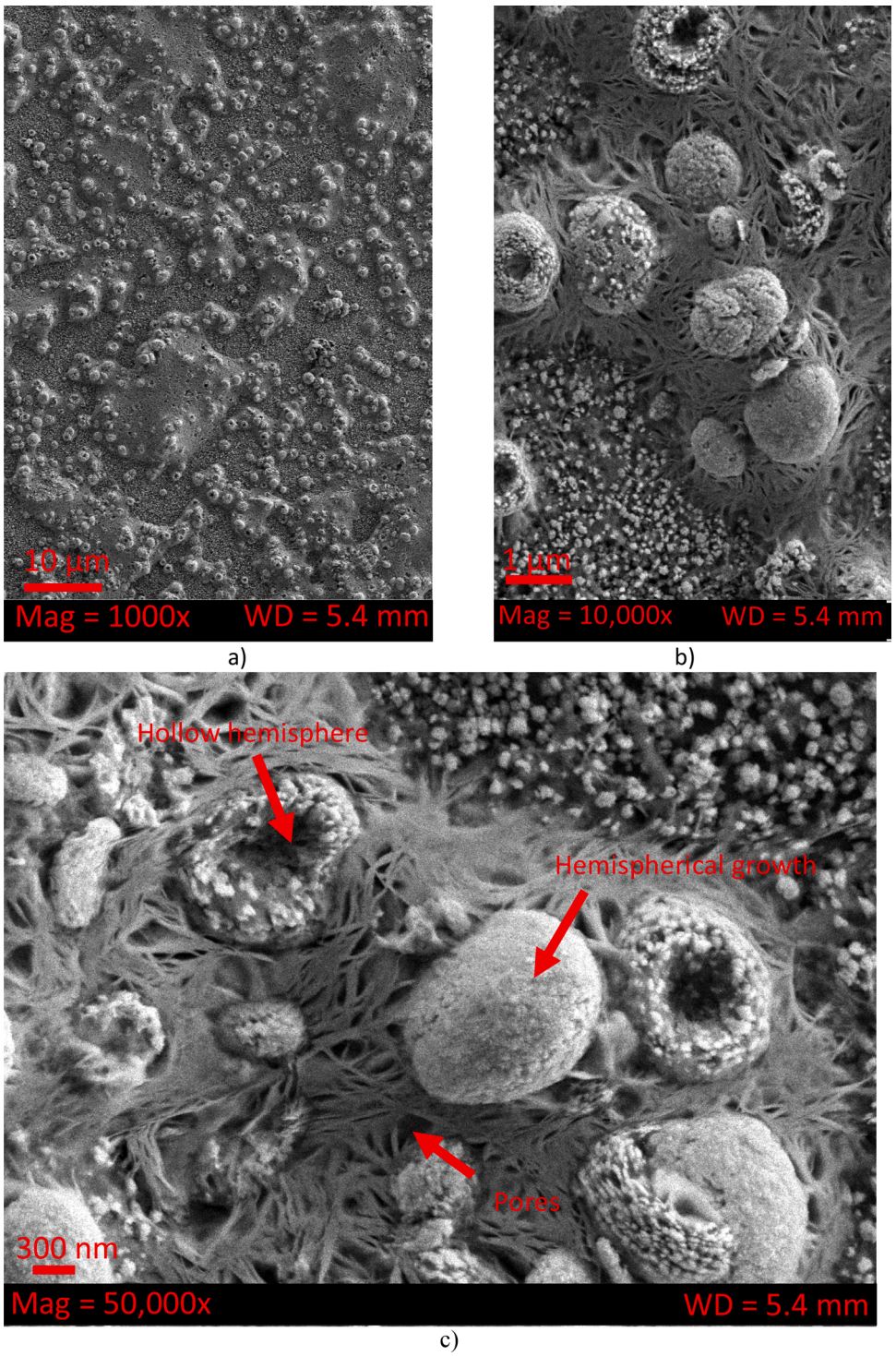

Fig. 10. FESEM Images of ZnO-HMT at various magnifications – a) 2000x magnification, b) 10,000x magnifications and c) 50,000 magnifications.

whole synthesis process. Various images of magnifications were recorded for both ZnO and its HMT enhanced counterpart. Maximum magnification allowed for each sample is at 50,000 kx and higher magnifications would result in blurred images and sample burn due to high intensity of electron propagations. Nanostructure of ZnO was seen to be slightly different when HMT was added. Due to the nature of ZnO material being conductive, coating with gold nanoparticles or other conductive materials is not required for the equipment to display clear imagery.

According to Fig. 9a) and b), it was observed that ZnO growth was leaning towards formation of nano-flakes when the low temperature hydrothermal method was applied. Formation of large islands is a result of irregular growth of the zinc oxide crystals. However, upon closer inspection with higher magnifications, Fig. 9c) shows creasing and rough surface sheets rather than sharp flake edges. The materials agglomerate or clump to each other forming irregular crease and islands. This is due to the result of low temperature annealing of ZnO [45]. The creasing and rough surface of the zinc oxide nano structure allows water droplets to adhere to the surface thus making the material capable of hygroscopic behaviours.

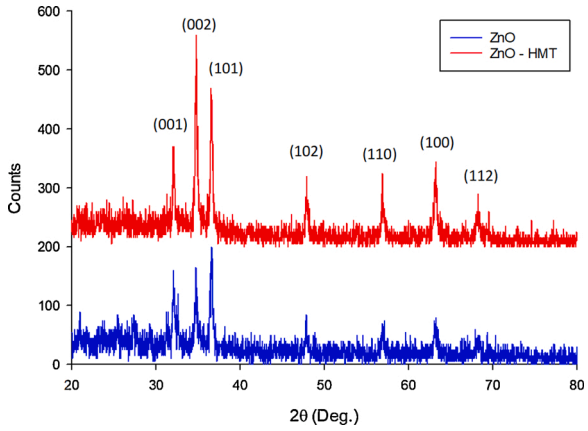

Fig. 11. XRD Spectra of ZnO and ZnO-HMT.

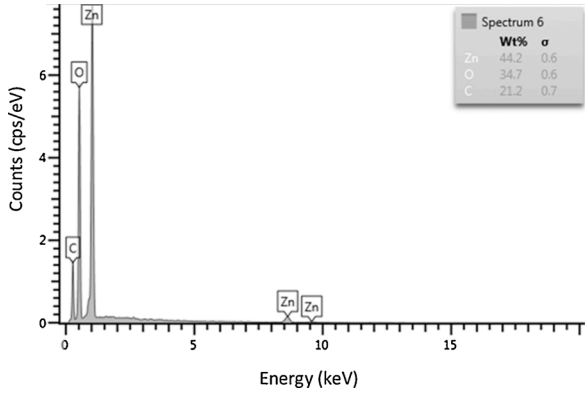

Fig. 12. Elemental analysis EDS spectra of ZnO.

Upon addition of the organic additive to the ZnO synthesis process, Fig. 10a) shows micro hemispherical crystal growths of ZnO crystals forming on the substrate. At higher magnifications as displayed in Fig. 10b) and c), the hemispherical crystal structure is also surrounded by nano-pores and thick web-like structures. Some of the hemispherical structures appears to have a large pore of their own as well. It is possible that these structural features enable more adhesion sites for water molecules to attach. A material is more hygroscopic when it can allow adsorption of water on its surface.

3.3. XRD crystallography

Brief crystal study has been done for validation that HMT does not cause significant deformation or introduce increased impurity to zinc oxide nanostructure. XRD analysis with CuKα radiation source confirms multiple peaks corresponding to the zinc oxide compound based on Fig. 11. Diffrac EVA software equipped with powder diffraction data matches the spectra of both materials to be in accordance with PDF-00-001-1136. The notable crystal peaks of (002), (101), (102), (110) and (100) are observed in both samples within 2theta scanning range of 20−80°. The spectra detected minimal unknown peaks suggesting the sample is close to being uncontaminated and zinc oxide crystal structure is holding together without being too amorphous or having unknown crystal structure.

When comparing both ZnO and ZnO-HMT sample spectra, it was observed that ZnO-HMT revealed higher peaks compared to its counterpart with no additive. The HMT additive managed to enhance the crystal bonds within the ZnO compounds that contributes to the crystal growth. This results in the detection of more diffracted X-ray and leads to an increase in peaks revealed. Peaks (001), (002) and (101) show a significant increase upon addition of the additive to the ZnO. These increments occur in crystals that experienced the increased growth rate. Despite the increase in the ZnO characteristic peaks, addition of HMT does not lead to extreme deformation of crystal or alterations in the crystal structures which explains why the ZnO-HMT peaks are almost similar with ZnO peaks 2θ angle wise.

3.4. Validation of analytical technique

Water uptake by the ZnO nanostructures are monitored by weighing on a sensitive mass scale. To ensure this analytical technique is reliable, based on Fig. 3, both the water uptake and water release effect on the weight values were plotted. Along with this, the FESEM images were also observed for any deformations due to the water uptake or release of the ZnO material. As FESEM only provides images of nanostructures, it is essential for application of energy dispersive x-ray spectroscopy (EDS) be added together with the FESEM imaging. This is to confirm that the nanostructure was composed of the expected elements.

Based on Figs. 12 and 13, both show dominant Zn and O elements which is expected since that is the only elements that were involved in this study. For Fig. 13 which corresponds to the HMT loaded ZnO, there

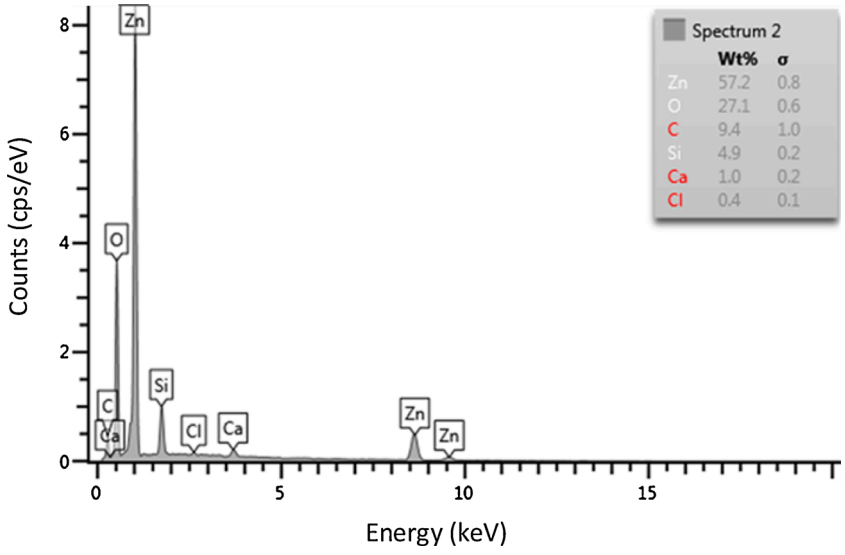

Fig. 13. Elemental analysis EDS spectra of HMT-ZnO.

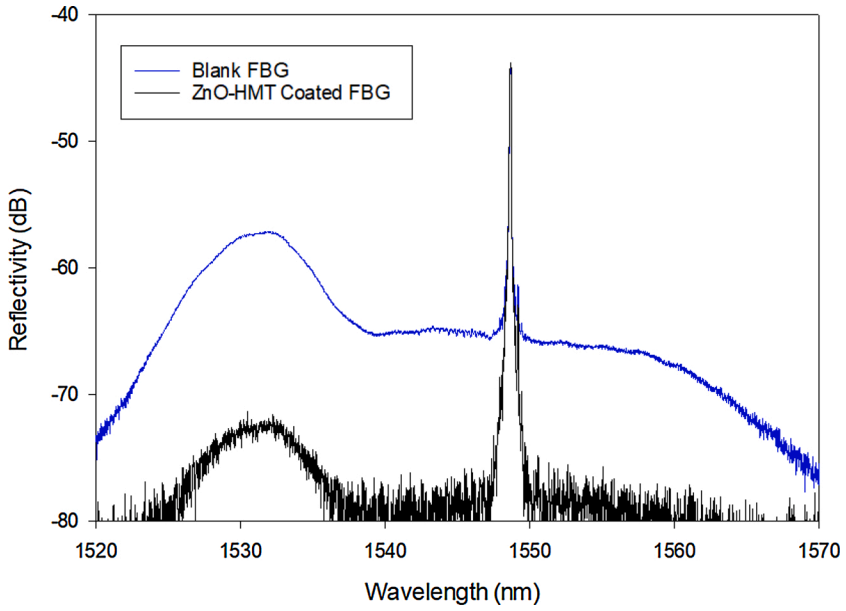

Fig. 14. Optical spectrum of blank fiber and ZnO-HMT coated fiber.

seems to be small peak of silica, Si due to the presence of porous structures. Since EDS utilizes x-ray, the dispersion may have reached to the substrate glass slide which is primarily made of Si. While Fig. 12 have no peaks referring to the Si element which means there was no pore present on the ZnO nano-creased sheets.

3.5. Implementation of ZnO-HMT onto FBG

The hydrothermally synthesized ZnO-HMT was coated onto a blank FBG. The FBG used in this study has Bragg grating implemented via phase masking technique [46] within 1550 nm wavelength with grating length of 10 mm. ZnO-HMT growth solution was coated via drop coating method onto the sensing region (where the FBG profile was imprinted). The solution was dropped 1 ml every minute until total of 10 ml of the solution was dropped on the FBG. Annealing at 70 °C was done after the coating stage. The coated FBG was connected within a circuit with amplified spontaneous emission broadband source, optical circulator and optical spectrum analyzer (OSA) for monitoring the reflectivity spectrum. The test was done in an open system and exposed to the room humidity which was recorded to be approximately 50 %RH and temperature of 28 °C.

Optical spectrum of FBG fiber is shown in Fig. 14. For comparative reason, the spectrum of the FBG fiber before it was coated was obtained. It was observed that the reflectivity spectrum was lower in the overall optical power compared to the uncoated FBG curve. However, similar power curves resulted from the broadband ASE was still visible and most importantly, the peak wavelength was not perturbed at all. The peak power at 1550 nm for the ZnO-HMT curve is nearly equal to that of blank FBG fiber. The purpose of this coating on FBG attempt was to examine whether there was a great disturbance on the 1550 nm peak upon coating. It was clearly observed that the peak and its power was not affected at all after the ZnO-HMT has been coated. This has shown the possibility of coating ZnO-HMT onto the FBG without impacting its Bragg peaks.

4. Conclusion and recommendation

All analysis had been performed on ZnO samples and its additive loaded counterpart. Based the morphological results, both samples are from different nanostructures of ZnO. The creased nanosheets of ZnO became hemispherical crystals when loaded with HMT at lower temperature hydrothermal synthesis. The differences between these samples has been further quantified with the weighing technique adapted from ASTM hygroscopic test technique. ZnO and ZnO-HMT both exhibits hygroscopic behaviour within humid and dry environment. The additive loaded ZnO have shown better hygroscopic via the weighing method by having a slightly steeper gradient compared to the original ZnO. The increase in gradient steepness correlates to how much water has been adsorbed onto the nanostructure surface upon increasing humidity. XRD analysis conforms that no elemental or distinct crystal structural changes occurred on ZnO when a heterocyclic additive has been added and synthesized at lower temperatures. Additionally, EDS was performed together with FESEM for elemental conformation on images and have shown that only Zn and O atoms are dominant in view. A low temperature synthesized; ZnO-HMT is potent to be used as a humidity sensor.

The applied technique carried out in this study bears favourable output to the extent that a material can be characterized as hygroscopic. However, it bears weakness that can however be improved in future studies. These gaps in the technique may help in producing more reliable or accurate results for material hygroscopic characterization. In weighing samples in the microbalance, it is favoured to have the chamber sealed as perfectly as possible. When the chamber is fully sealed, humidity may be able to be lower or higher depending on how much the RH contributor material present together with the sample inside the chamber itself. ZnO synthesis comes in various methods and most journals reported ZnO with well-shaped or uniform nanostructures involves annealing the material at much higher temperatures. Uniform and rougher nanostructures with higher surface areas are known to be able to exhibit better water absorbency. Therefore, for forming more quality and higher surface area nanostructures, high temperature of more than 200 °C may be favourable depending on the capability of an industry.

Author statement

M. A. Riza: Writing - Original Draft, Formal analysis, Validation, Investigation; Y.I. Go: Conceptualization, Methodology, Writing - Review & Editing, Supervision, Project administration; R.R.J. Maier: Conceptualization, Methodology, Supervision, Visualization; S. W. Harun: Resources; S. B. Anas: Resources.

Funding

The funding provider of this study is the Ministry of Higher Education Malaysia under the Fundamental Research Grant Scheme (FRGS), No. FRGS/1/2018/TK10/HWUM/02/2.

Declaration of Competing Interest

The authors declare that they have no competing interests.

Appendix A

Table A1

Table A1
Hygroscopic techniques.

Technique	Parameter Involved	Sample form	Ref.
Weighing method	• Weight of sample • Time of exposure • humidity manipulation • Open environment	Powders/thin film	[9]
Weighing method	• Weight of container • Weight of sample • Vacuum Environment • Time of exposure	Liquids/pigment	[10]
Simulation with real environment data	• Simulation with actual room • Microscopic observation	Actual room with environment data	[12]
Black-spot ratio count	• Black-spot count via microscope observation	Thin film layer of solar cell	[14]
Tandem nano-differential mobility analysis (TDMA)	• Particle size • Film thickness	Nano droplets	[13]
Microscopic observation + humidity sensing performance comparison	• Humidity manipulation • Film thickness • Pore sizes	Thin film	[15]
Microscopic observation	• Film thickness • Pore sizes • Nanoparticle diameters	Thin film	[16]
Microscopic observation	• Temperature • Pressure • Humidity manipulation	Powder	[17]
Sum of frequency generation spectroscopy (SFG)	• Chemical functional group • Microscopic observation	Thin film	[18]
Quartz crystal microbalance (QCM)	• Weight of sample	Thin film	[11]

References

[1] P.J. Thomas, J.O. Hellevang, A fully distributed fibre optic sensor for relative humidity measurements, Sens. Actuators B Chem. 247 (2017) 284–289, 2017/08/01/.
[2] S. Lee, J.-W. Park, Reversible humidity-driven tuning of the light scattering properties of PS:PEG-based porous polymer films: understanding derived from the cross-sensitivity of a luminescent oxygen sensor, Sens. Actuators B Chem. 298 (2019) 126883, 2019/11/01/.
[3] R.J. Mortimer, R.J. Mayes, Characterisation and humidity-sensing properties of aluminium (oxy)-hydroxide films prepared by cathodically induced precipitation, Sens. Actuators B Chem. 128 (1) (2007) 124–132, 2007/12/12/.
[6] S.R. Byrn, G. Zografi, X. Chen, Hygroscopic properties of solids. Solid State Properties of Pharmaceutical Materials, 2017, pp. 213–230, https://doi.org/10.1002/9781119264408.ch15 pp, 2017/06/30.
[7] D. Gouvêa, S.V. Ushakov, A. Navrotsky, Energetics of CO2 and H2O adsorption on zinc oxide, Langmuir 30 (30) (2014) 9091–9097, 2014/08/05.
[8] J.T. Newberg, C. Goodwin, C. Arble, Y. Khalifa, J.A. Boscoboinik, S. Rani, ZnO (101¯0) surface hydroxylation under ambient water vapor, J. Phys. Chem. B 122 (2) (2018) 472–478, 2018/01/18.
[9] Q. Zheng, S. Liu, S. Yang, J. Lei, X. Peng, C. Lin, Influence of insoluble substance hygroscopicity on insulator leakage current, 2016 IEEE International Conference on High Voltage Engineering and Application (ICHVE) (2016) 1–4.
[10] A.S.T.M. D280-01(2019), Standard Test Methods for Hygroscopic Moisture (and Other Matter Volatile Under the Test Conditions) in Pigments, 2019.
[11] B.D. Vogt, C.L. Soles, H.-J. Lee, E.K. Lin, W.-l. Wu, Moisture absorption into ultrathin hydrophilic polymer films on different substrate surfaces, Polymer 46 (5) (2005) 1635–1642, 2005/02/14/.
[12] H. Xie, G. Gong, Y. Wu, Y. Liu, Y. Wang, Research on the hygroscopicity of a composite hygroscopic material and its influence on indoor thermal and humidity environment, Appl. Sci. 8 (2018) 430, 03/13.
[13] A.C. MacMillan, T.M. McIntire, S.A. Epstein, S.A. Nizkorodov, Effect of alkyl chain length on hygroscopicity of nanoparticles and thin films of imidazolium-based ionic liquids, J. Phys. Chem. C 118 (50) (2014) 29458–29466, 2014/12/18.
[14] M. Kim, S.G. Motti, R. Sorrentino, A. Petrozza, Enhanced solar cell stability by hygroscopic polymer passivation of metal halide perovskite thin film, Energy Environ. Sci. 11 (9) (2018) 2609–2619, https://doi.org/10.1039/C8EE01101J.
[15] J.-G. Liang, E.-S. Kim, C. Wang, M.-Y. Cho, J.-M. Oh, N.-Y. Kim, Thickness effects of aerosol deposited hygroscopic films on ultra-sensitive humidity sensors, Sens. Actuators B Chem. 265 (2018) 632–643, 2018/07/15/.
[16] X. Zhang, J. He, Antifogging antireflective thin films: does the antifogging layer have to Be the outmost layer? Chem. Commun. 51 (2015), 06/30.
[17] M. Ebert, M. Inerle-Hof, S. Weinbruch, Environmental scanning electron microscopy as a new technique to determine the hygroscopic behaviour of individual aerosol particles, Atmos. Environ. 36 (39) (2002) 5909–5916, 2002/12/01/.
[18] E. Hsiao, A.L. Barnette, L.C. Bradley, S.H. Kim, Hydrophobic but hygroscopic polymer films – identifying interfacial species and understanding water ingress behavior, ACS Appl. Mater. Interfaces 3 (11) (2011) 4236–4241, 2011/11/23.
[19] S. Réquilé, A. Le Duigou, A. Bourmaud, C. Baley, Interfacial properties of hemp fiber/epoxy system measured by microdroplet test: effect of relative humidity, Compos. Sci. Technol. 181 (2019) 107694, 2019/09/08/.
[20] L. Roedel, V. Bednarzig, R. Belli, A. Petschelt, U. Lohbauer, J. Zorzin, Self-adhesive resin cements: pH-neutralization, hydrophilicity, and hygroscopic expansion stress, Clin. Oral Investig. 21 (5) (2017) 1735–1741, 2017/06/01.
[21] R. Nomoto, J.F. McCabe, A simple acid erosion test for dental water-based cements, Dent. Mater. 17 (1) (2001) 53–59, 2001/01/01/.
[22] Y.-j. Wei, N. Silikas, Z.-t. Zhang, D.C. Watts, Hygroscopic dimensional changes of self-adhering and new resin-matrix composites during water sorption/desorption cycles, Dent. Mater. 27 (3) (2011) 259–266, 2011/03/01/.
[23] A. Sridharan, K. Prakash, S. Sudheendra, Hygroscopic moisture content: determination and correlations, Environ. Geotech. 3 (2014), 01/01.
[24] M. Law, L.E. Greene, J.C. Johnson, R. Saykally, P. Yang, Nanowire dye-sensitized solar cells, Nat. Mater. 4 (6) (2005) 455–459, 2005/06/01.
[25] S.H. Ko, et al., Nanoforest of hydrothermally grown hierarchical ZnO nanowires for a high efficiency dye-sensitized solar cell, Nano Lett. 11 (2) (2011) 666–671, 2011/02/09.
[26] S. Palit, K. Singh, B.-S. Lou, J.-L. Her, S.-T. Pang, T.-M. Pan, Ultrasensitive dopamine detection of indium-zinc oxide on PET flexible based extended-gate field-effect transistor, Sens. Actuators B Chem. 310 (2020) 127850, 2020/05/01/.
[27] A. Scandurra, E. Bruno, G.G. Condorelli, M.G. Grimaldi, S. Mirabella, Microscopic model for pH sensing mechanism in zinc-based nanowalls, Sens. Actuators B Chem. 296 (2019) 126614, 2019/10/01/.
[28] Y.V. Kaneti, et al., Experimental and theoretical studies of gold nanoparticle decorated zinc oxide nanoflakes with exposed {101¯0} facets for butylamine sensing, Sens. Actuators B Chem. 230 (2016) 581–591, 2016/07/01/.
[29] G.N. Narayanan, K. Annamalai, Role of hexamethylenetetramine concentration on structural, morphological, optical and electrical properties of hydrothermally grown zinc oxide nanorods, J. Mater. Sci. Mater. Electron. 27 (2016), 07/21.
[30] A. Mohamad Aris, Tapered Fiber Bragg Grating Sensor Coated With Zinc Oxide Nanostructures for Humidity Measurement, 2017, pp. 1–5.
[31] M.Y.A. Rahman, A.A. Umar, L. Roza, M.M. Salleh, Effect of hexamethylenetetramines (HMT) surfactant concentration on the performance of TiO2 nanostructure photoelectrochemical cells, Russ. J. Electrochem. 50 (10) (2014) 974–980, 2014/10/01.
[32] X. Wang, et al., Dispersed WO3 nanoparticles with porous nanostructure for ultrafast toluene sensing, Sens. Actuators B Chem. 289 (2019) 195–206, 2019/06/15/.
[33] S.E.H. Etaiw, D.M. Abd El-Aziz, S.N. Abdou, Single crystal of new nanostructure self-assembled copper–Cyanide and Hexamethylenetetramine as an efficient supramolecular coordination polymer catalyst, J. Inorg. Organomet. Polym. Mater. 28 (3) (2018) 1136–1148, 2018/05/01.
[34] A. Umar, A.A. Alshahrani, H. Algarni, R. Kumar, CuO nanosheets as potential scaffolds for gas sensing applications, Sens. Actuators B Chem. 250 (2017) 24–31, 2017/10/01/.
[35] D. Han, L. Zhai, F. Gu, Z. Wang, Highly sensitive NO2 gas sensor of ppb-level detection based on In2O3 nanobricks at low temperature, Sens. Actuators B Chem. 262 (2018) 655–663, 2018/06/01/.
[36] A.K. Gupta, et al., Au-spotted zinc oxide nano-hexagonrods structure for plasmon-photoluminescence sensor, Sens. Actuators B Chem. 290 (2019) 100–109, 2019/07/01/.

[37] N. Caicedo, R. Leturcq, J.-P. Raskin, D. Flandre, D. Lenoble, Detection mechanism in highly sensitive ZnO nanowires network gas sensors, Sens. Actuators B Chem. 297 (2019) 126602, 2019/10/15/.
[38] C.M. Chang, M.H. Hon, I.C. Leu, Preparation of ZnO nanorod arrays with tailored defect-related characterisitcs and their effect on the ethanol gas sensing performance, Sens. Actuators B Chem. 151 (1) (2010) 15–20, 2010/11/26/.
[39] H. Kim, Y. Pak, Y. Jeong, W. Kim, J. Kim, G.Y. Jung, Amorphous Pd-assisted H2 detection of ZnO nanorod gas sensor with enhanced sensitivity and stability, Sens. Actuators B Chem. 262 (2018) 460–468, 2018/06/01/.
[40] T. Wang, et al., Microwave preparation and remarkable ethanol sensing properties of ZnO particles with controlled morphologies in water-ethylene glycol binary solvent system, Sens. Actuators B Chem. 255 (2018) 1006–1014, 2018/02/01/.
[41] S. Patra, et al., Optical, structural properties and antibacterial activities of uncapped and HMT capped ZnO nanoparticles, Mater. Today Commun. 12 (2017) 133–145, 2017/09/01/.
[42] F. Gobo, T. Goto, T. Long, S. Yin, T. Sato, Mild solution synthesis of plate-like and rod-like ZnO crystals, Res. Chem. Intermed. 37 (2) (2011) 211–217, 2011/04/01.
[43] M. Abdullah, N. Bidin, G. Krishnan, M.F.S. Ahmad, M. Yasin, Fiber optic radial displacement sensor-based a beam-through technique, IEEE Sens. J. 16 (2) (2016) 306–311.
[44] M. Caponero, R. D'Amato, A. Polimadei, G. Terranova, Polymer-coated FBG humidity sensors for monitoring cultural heritage stone artworks, Measurement 125 (2018) 325–329, 2018/09/01/.
[45] S. Shaziman, A.S. Ismail@rosdi, M.H. Mamat, A.S. Zoolfakar, Influence of growth time and temperature on the morphology of ZnO nanorods via hydrothermal, in: IOP Conference Series: Materials Science and Engineering, vol. 99, 2015, p. 012016, 2015/11/19.
[46] R. Oliveira, L. Bilro, T.H.R. Marques, C.M.B. Cordeiro, R. Nogueira, Simultaneous detection of humidity and temperature through an adhesive based Fabry–Pérot cavity combined with polymer fiber Bragg grating, Opt. Lasers Eng. 114 (2019) 37–43, 2019/03/01/.

Muhammad Arif Riza received a B.Eng. in chemical engineering from MARA University Institute of Technology, Malaysia in 2015. He then received his Master of Science in renewable energy from the National University of Malaysia in 2019. He is registered as graduate engineer under Board of Engineers Malaysia. Currently, he is pursuing PhD under School of Engineering and Physical Sciences, Heriot-Watt University Malaysia. He focuses on developing new nanostructure compositions for chemical and environmental sensing, hydrodynamics of materials and new nanostructure coating via chemical synthesis techniques. His project also involves new etching technique for partial removal of fiber via chemical process to enhance the sensitive of fiber Bragg grating sensor. His research interests also include advanced photovoltaic materials, semiconductors and fibre optic sensing nanostructures.

Yun Ii Go holds Doctor of Philosophy in Engineering, Master of Science in Engineering and Bachelor of Engineering in Electrical & Electronics. She is passionate in sustainable development and green technology for resilient living. She is currently an Associate Professor with the School of Engineering and Physical Science, Heriot-Watt University Malaysia. She led as principal investigator and key researcher in multiple research projects including funding from Energy Academy, Royal Academy of Engineering UK, Ministry of Education Malaysia, Ministry of Foreign Affair Taiwan and Global Challenge Research Fund. She is a Chartered Engineer of Institution of Engineering and Technology (IET), senior member of Institute of Electrical and Electronics Engineers (IEEE) and The Optical Society (OSA).

Sulaiman Wadi Harun received a B.E. degree in electrical and electronics system engineering from the Nagaoka University of Technology, Nagaoka, Japan, in 1996, and the M. Sc. and Ph.D. degrees in photonics from the University of Malaya, Kuala Lumpur, Malaysia, in 2001 and 2004. Currently, he is a Full Professor with the Faculty of Engineering. He is an expert in fibre optic active and passive devices. He has nearly 20 years of research experiences on the development of optical fiber devices including fiber amplifiers, fiber lasers and fiber optic sensors. Prof. Harun has published more than 700 articles in ISI journals and his papers have been cited more than 6500 times with an h-index of 33, showing the impact on the community. He has successfully supervised more than 50 PhD students to completion. He received a prestigious award of Malaysian Rising Star 2016 from the Ministry of Higher Education Malaysia for his contribution in international collaboration.

Robert Maier received the Dipl.Ing.FH degree in 1980 and the Ph.D. degree in physics, focusing on the applications of FBGs in sensors, in 2006 from Heriot-Watt University, Edinburgh, United Kingdom. He conducted research on instrumentation in nuclear medicine and ophthalmology before joining the Max Plank Institute for Quantum Optics, München, Germany, in 1982 as a Lab Engineer, where he worked on laser technology and experimental instrumentation. In 1985, he joined Technolas Lasertechnik as a Research and Development Manager in Excimer lasers for medical applications. In 1987, he moved to the FORTH Institute, Crete, to develop laser plasma based analytical techniques for gold ore analysis. He continued this research after his move in 1988 to Edinburgh University, Chemistry, where he expanded his research into a wide range of spectroscopic instrumentation. In 1998, he joined the Applied Optics Group, Department of Physics, Heriot-Watt University, Edinburgh, to work on fiber optic beam delivery of high-power lasers, where he focused on fiber optic sensor technology. He was a Visiting Professor from the Hochschule München University for Applied Sciences where he lectured on optoelectronic instrumentation in 2012. His research focuses on fiber optic sensor technology in engineering applications, using FBGs, interferometric sensing techniques and environmental sensing using Pd thin films (for hydrogen sensing). His current research interests include sensing in extreme environments and embedded sensing in structures manufactured by additive layer manufacturing techniques in polymeric materials and metallic systems using high temperature compatible fiber sensors, such as regenerated fiber Bragg gratings and interferometry to facilitate the use of optical sensors at high temperatures and to permit strain and condition monitoring from within a metallic structure.

Siti Barirah Ahmad Anas received the B.Eng. degree (Hons.) in computer and electronic systems from the University of Strathclyde, U.K., in 1999, the M.Sc. degree in communication and network engineering from Universiti Putra Malaysia, Malaysia, in 2003, and the Ph.D. degree in electronic systems engineering from the University of Essex, U.K., in 2009. She is currently an Associate Professor with the Faculty of Engineering, University Putra Malaysia. Her current research interests include optical transmission systems, optical multiplexing techniques, and optical access network technologies. She actively involved in the Institute of Electronics and Electrical Engineering (IEEE) by serving as the executive committee in IEEE Photonics Society Malaysia Chapter for many years.